Composites

Preparation and characterization of glass fiber/polyimide/SiO₂ composite aerogels with high specific surface area

Zhifang Fei[1,2,*] , Zichun Yang[1,2], Guobing Chen[1,2], Kunfeng Li[1,2], Shuang Zhao[1,2], and Gaohui Su[3]

[1] School of Power Engineering, Naval University of Engineering, Wuhan 430033, Hubei, China

[2] Institute of High Temperature Structural Composite Materials of Naval Ship, Naval University of Engineering, Wuhan 430033, Hubei, China

[3] 3 Unit 91663 of Navy, Qingdao 266000, Shandong, China

ABSTRACT

A glass fiber/polyimide (PI)/SiO₂ composite aerogel (FPS aerogel) was prepared by dispersing glass fibers in PI/SiO₂ hybrid sol derived from 4,4′-oxydianiline (ODA), pyromellitic dianhydride (PMDA) and tetraethoxysilane (TEOS) with supercritical CO₂ fluid drying technology. The SiO₂ primary particles were combined with PI chains which improved the strength of the composite aerogel, and the glass fibers inhibited the shrinkage deformation during the drying process by acting as the supporting skeletons. Effects of PI contents on the density, shrinkage, thermal conductivity and mechanical properties of the FPS aerogels were investigated. The as-prepared FPS aerogels had low densities (0.116–0.145 g/cm^3), high specific surface area (844–963 m^2/g), low thermal conductivity (0.0268–0.0280 W m^{-1} K^{-1} at room temperature) and relatively high compression strength (0.12–0.29 MPa) with integrated nanostructures, fewer powders and stronger fiber/aerogel matrix interfaces. The density, the shrinkage, the thermal conductivity and the compression strength of the FPS aerogels increased with the increasing PI content. This research provided a new method employing PIs and glass fibers as strengthening phases to improve the mechanical properties of SiO₂-based aerogels.

Introduction

SiO₂ aerogel is a lightweight multi-functional porous material with continuous porosity and nanostructures composed of numerous nanoscale particles [1, 2]. The unique properties of SiO₂ aerogels include low density, high porosity, high specific surface area, low acoustic velocity and low thermal conductivity. These properties suggest promising application of SiO₂ aerogels for thermal insulation [3], sound insulation [4]

---

and absorption material [5]. However, in the unique high-porosity three-dimensional structure of SiO_2 aerogels, the weak bonding force between solid phase particles result in their poor mechanical properties, such as low strength, significant brittleness and fragility. Consequently, the direct applications of SiO_2 aerogels are limited. On the one hand, SiO_2 aerogels are enhanced by optimizing the preparation process, such as aging process. The structures and properties of SiO_2 aerogels prepared under different aging conditions are studied [6, 7]. On the other hand, the mechanical properties of aerogels are improved by the introduction of reinforcing phases, and the more common modification methods are either fiber reinforcement [8–14] or polymer cross-linking [15–19]. The former is a physical modification method where the fibers act as the supporting skeletons and are uniformly dispersed in a silica sol. The latter is a chemical modification method on the molecular scale where the polymer molecular chains are grafted to the surface of the SiO_2 primary particles. Both methods have advantages and disadvantages. For example, the composite aerogels prepared by the method of fiber reinforcement have large specific surface areas and high porosity; however, they are easy to powder and both the compression strength and Young's modulus are relatively small. Many reports have studied SiO_2-based composite aerogels prepared using the glass fiber as a strengthening phase. However, the compressive properties of these composite aerogels are generally low, and the value of Young's modulus is only 0.5 MPa (0.12 g/cm^3) [9] or 0.41–1.03 MPa (0.13–0.16 g/cm^3) [10]. For the method of polymer cross-linking modification, the mechanical properties of the polymer cross-linked SiO_2 aerogels are excellent; however, the shrinkage during the drying process is large, contributing to the increasing density. The compressive property of SiO_2 aerogel can be significantly improved via polyimide (PI), for instance, as a strengthening phase, which has a significant application prospect with excellent thermal stability, thermal oxidation resistance and mechanical properties. The PI cross-linked SiO_2 aerogels have good mechanical properties with the Young's modulus of 5.4 MPa (0.28 g/cm^3) [15], 2–17 MPa (0.141–0.172 g/cm^3) [4] and 21.70–44.16 MPa (0.132–0.187 g/cm^3) [20]. However, the specific surface area of such materials is generally low (504 m^2/g [15], 463.2–582.7 m^2/g [4]), and the density (0.28 g/cm^3 [15]) and shrinkage (30.67% [15], 15.8–25.5% [20]) are higher compared to the fiber-

reinforced SiO_2 aerogel, which may adversely affect these properties. For instance, the thermal conductivity of PI cross-linked SiO_2 aerogel (0.0306–0.0347 at room temperature (0.132–0.187 g/cm^3) [20]) is higher than that of the fiber-reinforced SiO_2 aerogel (0.023–0.027 W m^{-1} K^{-1} at room temperature, 0.13–0.16 g/cm^3) [10]). In general, the introduction of PI leads to greater shrinkage of the hybrid wet gel in drying process, resulting in increased density of the PI cross-linked SiO_2 aerogel. And the density is directly linked with improvement of mechanical properties and the thermal conductivity. So fibers can be used to reduce the shrinkage deformation and the density of the PI cross-linked SiO_2 aerogel.

Herein, for the first time, the FPS aerogels were prepared by combining fiber reinforcement and PI cross-linking. PI chains were successfully combined with SiO_2 primary particles through a cross-linking reaction, which improved the aerogel strength. In addition, the glass fibers were inlaid in the aerogel matrix and were used as the supporting skeletons to strengthen the aerogel matrix and effectively inhibit the shrinkage deformation during the drying process.

Materials and methods

Materials

Tetraethoxysilane (TEOS, AR), pyromellitic dianhydride (PMDA, AR), 4,4'-oxydianiline (ODA, AR), 3-aminopropyltriethoxysilane (APTES, AR), 1-methyl-2-pyrrolidone (NMP, AR), pyridine (AR), ammonium hydroxide solution (28.0–30.0%, NH_3 basis), hydrochloric acid (HCl, AR) and ethanol (EtOH, AR) were purchased from Aladdin Industrial Corporation, China. Acetic anhydride (AR) was purchased from Sinopharm Chemical Reagent Cor. Ltd, China. Glass fiber (diameter 7 μm, length 3 mm) was purchased from Wuxi Xingxiao Insulation Materials Co., Ltd. Supercritical drying was performed using liquid carbon dioxide (industrial grade) which was purchased from Wuhan Shu Xing Gas Cor. Ltd, China.

The preparation of FPS aerogels

ODA (0.018 g) was dissolved in a beaker containing 40 ml NMP, and 0.039 g PMDA was then slowly added to the beaker. The mixed solution was stirred

for 3 h at room temperature. Then, 0.043 ml APTES was added and end capped with polyamic acid for 1 h. 0.137 ml acetic anhydride and 0.117 ml pyridine were added and stirred for 10 min to perform the chemical imidization process. 10.17 ml TEOS, 3.24 ml deionized water and HCl were added sequentially to the beaker. The PI/SiO_2 hybrid sol was obtained after the solution was placed in a water bath at 50 °C for 4 h. The molar ratio was ODA:PMDA:APTES = 1:2.01:2.02, TEOS:H_2O:HCl = 1:4:0.036. HCl was used to catalyze the hydrolysis process and the reaction was stirred at 50 °C for 3 h. After hydrolysis, a mixture of ammonium hydroxide and NMP (8 mol/L) was slowly added until the pH value was 7.0. Then, the chopped glass fibers (0.028 g) were added to the sol. The mixture was then continuously stirred at 50 °C with a stirring speed of 180 RPM to ensure relatively uniform dispersion of the fibers until the viscosity significantly increased and then poured into a polytetrafluoroethylene mold. The fiber/PI/SiO_2 gels were obtained after gelation within 20 min. After aging for 12 h, the gels were removed from the mold, and the solvent within the gels was exchanged with EtOH 3 times (for 12 h each time). Then, the wet gels were placed in a supercritical fluid extraction chamber filled with EtOH and exchanged with supercritical CO_2 at 10 MPa and 50 °C for 72 h. Finally, the FPS aerogel with 2 wt% PI and 1 wt% glass fibers named 1#_PI-2 wt%_GF-1 wt% was obtained after gaseous CO_2 was slowly released out from the chamber over 12 h. The PI-2 wt% or GF-1 wt% represented the mass fraction of the PI or glass fiber in the FPS aerogel. Figure 1 shows the preparation process and principle of the FPS aerogels. The chemical composition of FPS aerogels with different mass fraction of PI and the glass fibers is presented in Table 1.

Characterization

The chemical composition of the sample confirmed by a NICOLET 5700 FTIR Spectrometer Fourier transform infrared spectrometer. The microstructure of the sample was observed via a Hitachi SU8010 field emission scanning electron microscope. The sample was sprayed for 30 s, and the sputtering current was 10 mA. The aerogel samples were analyzed for specific surface area and pore size using a ASAP 2020 surface area analyzer at 77 K. An MTS Criterion Model 45 Electronmechanical Universal Testing System was used to test the compressive properties of the aerogels with a constant loading speed of 1.5 mm/min. The samples are cylindrical with size of about 18 mm in diameter and 30 mm in length. The top and bottom surfaces of samples are smoothly polished and in parallel. The thermal conductivity was calculated via the transient hot wire method at 25 °C in air using a thermal conductivity tester (TC3000, XIATECH, China). Thermogravimetric-differential thermal analysis was performed on a Setaram Labsys Evo thermal analyzer in air from 30 to 800 °C. The linear shrinkage (%) of the FPS aerogels throughout the drying process was taken as the difference between the diameters of the FPS aerogel monoliths and that of the wet gel divided by the diameter of the wet gel. The volume fraction of the fibers in the FPS aerogel can be calculated with the following formula.

$$\varphi\% = \frac{m}{\rho V} \tag{1}$$

The $\varphi\%$, m, ρ and V are the volume fraction of fibers in the FPS aerogel, the mass of fibers, the density of the fibers (2.2 g/cm^3) and the volume of the FPS aerogel.
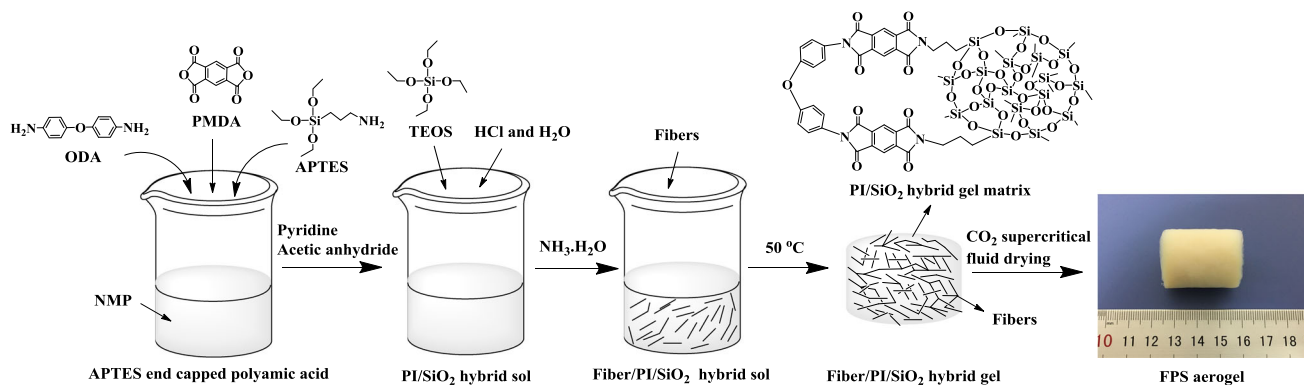
**Figure 1** The preparation process and principle of the FPS aerogels.

Table 1 The chemical composition of FPS aerogels with different mass fractions of PI and the glass fibers

Samples	PI/ wt%	Fiber/ wt%	TEOS (ml)	H₂O (ml)	ODA (g)	PMDA (g)	APTES (ml)	Pyridine (ml)	Acetic anhydride (ml)	Fiber (g)
1#_PI-2 wt%_GF-1 wt%	2	1	10.17	3.24	0.018	0.039	0.043	0.117	0.137	0.028
2#_PI-2 wt%_GF-2 wt%	2	2	10.17	3.24	0.018	0.039	0.043	0.117	0.137	0.057
3#_PI-2 wt%_GF-3 wt%	2	3	10.17	3.24	0.018	0.039	0.043	0.117	0.137	0.086
4#_PI-5 wt%_GF-1 wt%	5	1	10.17	3.24	0.046	0.101	0.110	0.302	0.354	0.030
5#_PI-10 wt%_GF-1 wt%	10	1	10.17	3.24	0.099	0.216	0.235	0.646	0.756	0.032

Results and discussion

Figure 2 shows the FPS aerogels with different weight percentages of PIs and fibers. The samples are light, yellow and cylindrical solid materials with smooth surfaces and no cracks. The samples won't drop the powder when they are touched. The samples maintain the shape before drying, and the fibers are evenly dispersed. After the introduction of the PI and the fiber, the FPS aerogels still maintain a low density and shrinkage.

Table 2 shows the parameters such as gelation time, shrinkage, volume fraction of fibers and density of samples with different proportions. The shrinkage, density and gelation time of FPS aerogels with the same fiber content (1 wt%) increase with the increasing PI content. The shrinkage of FPS aerogels is about 9.1–13.7%, which is lower compared to
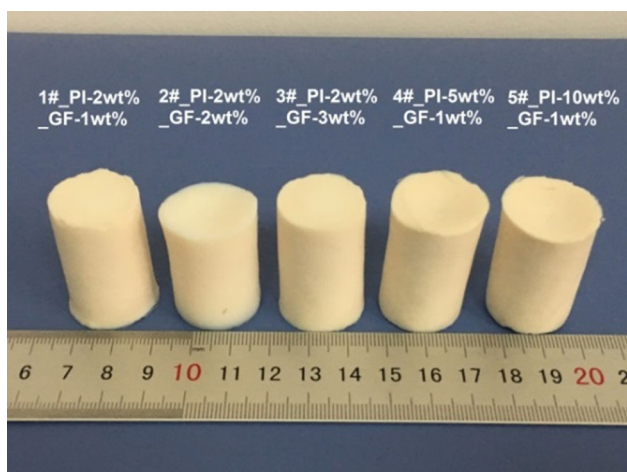
**Figure 2** FPS aerogel samples with different proportions.

reported PI cross-linked SiO₂ aerogels (23.84–30.67% [15] and 10.8–19.9% [4]). Additionally, the shrinkage of samples with the same PI content (2 wt%) decreases with the increasing fiber content, indicating that the fibers effectively inhibit the shrinkage of samples during the preparation process.

Three samples at each PI and fiber contents were prepared, and thermal conductivity values of these samples were tested three times at room temperature. As shown in Fig. 3, the average thermal conductivity is 0.0265–0.0282 W m⁻¹ K⁻¹. The low thermal conductivity has a close relationship with the unique three-dimensional network nanostructures of FPS aerogels. Specifically, the nanoscale skeleton of the aerogel greatly extends the heat conduction path and the gas conduction heat transfer in the pore is sufficiently suppressed because the pore size is mostly smaller than the mean free path of free air (70 nm). The thermal conductivity of FPS aerogels with the same fiber content (1 wt%) increases with the increasing PI content. This is because the increase in the PI content causes the increase in the density of the FPS aerogel, which leads to the increase in the solid heat conduction.

Figure 4 shows the FTIR spectra of the FPS aerogels (1#_PI-2 wt%_GF-1 wt%, 5#_PI-10 wt%_GF-1 wt%). The peaks at 1083, 796 and 458 cm⁻¹ all represent Si–O–Si bond of silica [21]. The peaks at 1778 and 1723 cm⁻¹ are attributed to the symmetrical and asymmetrical stretch vibrations of the imide C=O, and the peak at 1380 cm⁻¹ corresponds to the stretch vibration of C–N–C in the imide [4]. The peak at 1500 cm⁻¹ is attributed to the vibration absorption of benzene ring. The peaks at 2983 and 2905 cm⁻¹

**Table 2** Component, volume fraction of fibers, shrinkage, density and gelation time of FPS aerogels

Samples	Volume fraction of fibers/%	Linear shrinkage/%	Density/(g/cm^3)	Gelation time/min
1#_PI-2 wt%_GF-1 wt%	0.095	10.0	0.120	30
2#_PI-2 wt%_GF-2 wt%	0.187	9.7	0.124	35
3#_PI-2 wt%_GF-3 wt%	0.282	9.1	0.116	40
4#_PI-5 wt%_GF-1 wt%	0.103	10.6	0.132	52
5#_PI-10 wt%_GF-1 wt%	0.123	13.7	0.145	90
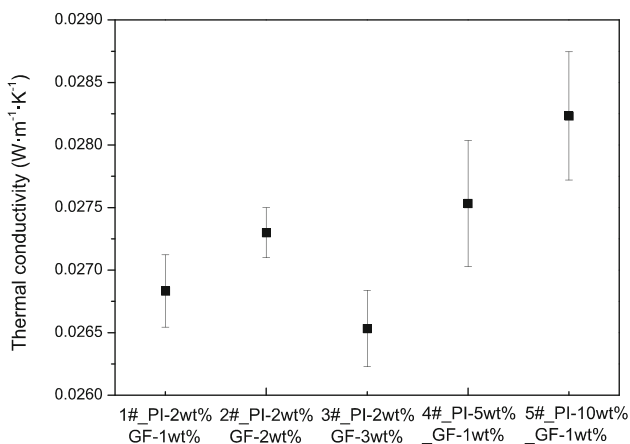
Figure 3 Thermal conductivity of the FPS aerogel.

correspond to either the residual non-hydrolyzed methoxysilane groups (–OC$_2$H$_5$) or the exchange solvent (ethanol) [22]. The peak at 3454 cm^{-1} is mostly attributed to the adsorbed water.

Figure 5 shows the SEM micrographs of aerogel sample numbered 4#_PI-5 wt%_GF-1 wt%. From Fig. 5a, b, we can see the fracture surface of the
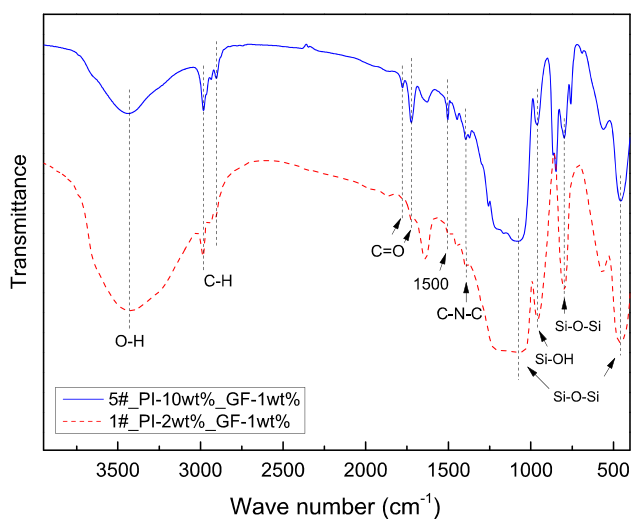

Figure 4 FTIR spectrum of the FPS aerogel.

sample composed of the PI/SiO$_2$ hybrid aerogel matrix and fibers. The diameter of the fiber is about 7 μm. The fiber as the skeleton of the material is interspersed in the aerogel matrix to reinforce the microstructure and to resist the shrinkage and the deformation. Both Fig. 5c, d indicates that the fibers are closely bound to the aerogel matrix without agglomeration and entanglement. Figure 5e demonstrates that the fiber surface is tightly wrapped by the aerogel matrix, which guarantees the strong combination of two phase interfaces. Figure 5f shows the microstructure of PI/SiO$_2$ hybrid aerogel matrix, which has a three-dimensional network composed of typical spherical particles. The sizes of the pore structures and the particles are at the nanometer scale, and the contact areas between the particles and the diameters of particles are larger compared to the pure SiO$_2$ aerogels. This is because that the particles have been combined with the PI via covalent bonds. And the PI will be beneficial for the improvement of the compressive properties of the composite aerogels.

Figure 6 shows the typical nitrogen adsorption–desorption isotherms of the FPS aerogels (1#_PI-2 wt%_GF-1 wt%, 2#_PI-2 wt%_GF-2 wt%, 4#_PI-5 wt%_GF-1 wt%, 5#_PI-10 wt%_GF-1 wt%). The adsorption isotherms slowly increase at low relative pressure ($P/P_0 < 0.8$) and r significantly increases at high relative pressure ($P/P_0 > 0.8$). According to the classification of adsorption isotherms proposed by International Union of Pure and Applied Chemistry (IUPAC), the adsorption isotherms are type IV curves. This type of adsorption curve shows that the aerogels have mesopores with sizes in the range of 2–50 nm.

Figure 7 shows the pore size distributions of the aerogels. The pore size distribution peaks at about 30–45 nm, but trails out to about 100 nm. Table 3 shows the specific surface area, pore volume, average pore size and other parameters of the aerogel calculated by the BET method. The specific surface area of
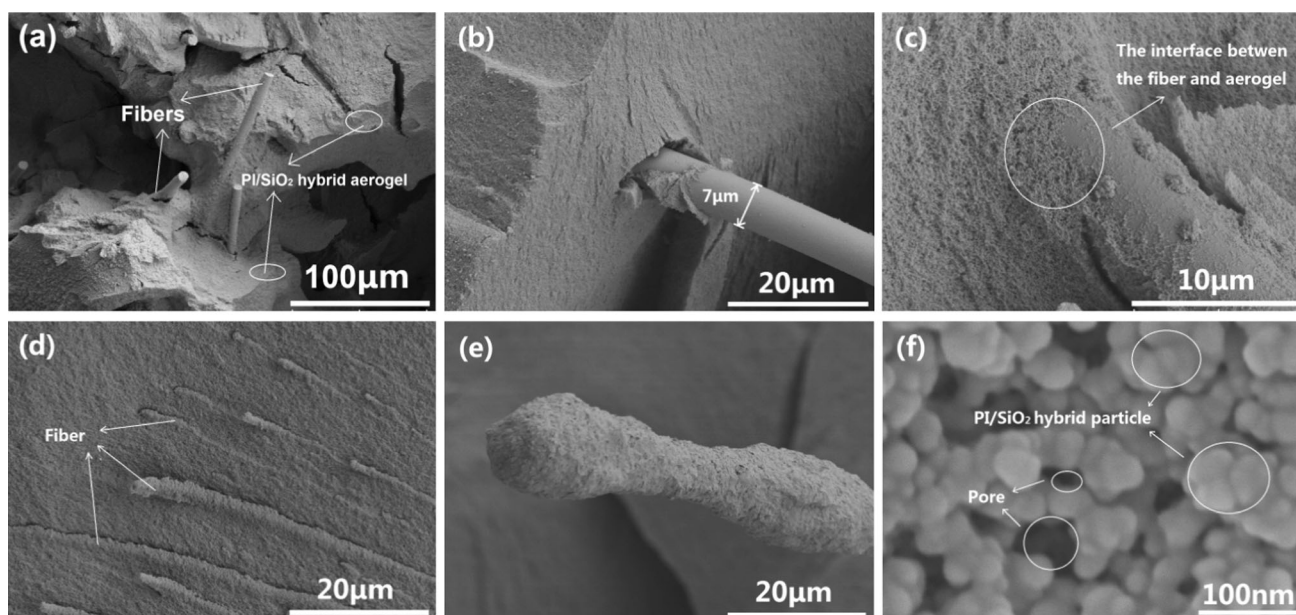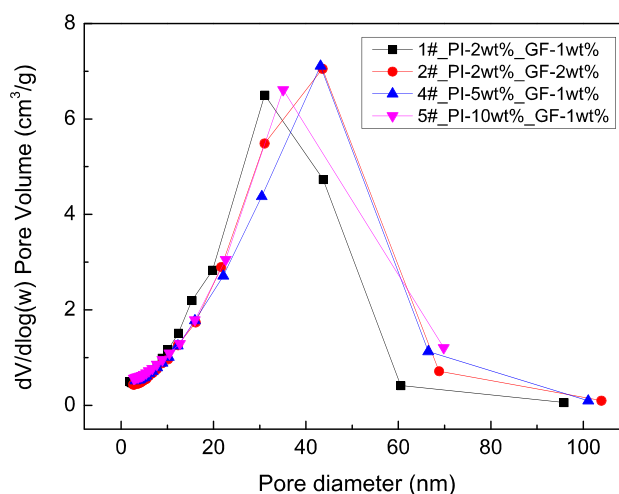
Figure 5 SEM micrographs of the FPS aerogel.
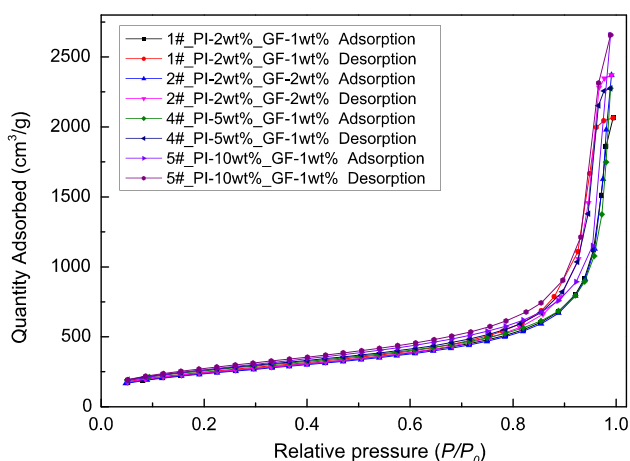
Figure 6 N$_2$ adsorption–desorption isotherms of FPS aerogels.

Figure 7 Pore size distributions of FPS aerogels.

aerogels with different compositions ranges from 844 to 963 m^2/g. The high specific surface area indicates that the aerogel maintains the integrity of nanostructure during the preparation and the drying of the wet gel. This is attributed to the introduction of the PI which significantly strengthens the skeleton structure of the SiO$_2$ matrix. And the introduction of the fiber effectively inhibits the shrinkage deformation during the drying process, enabling the FPS aerogel to retain the identical high specific surface area and mesoporous form as the pure SiO$_2$ aerogel.

Figure 8 shows the typical stress–strain curves of the FPS aerogels with different PI contents. The fiber content of all three samples is 1 wt%, and the content

of PI is 2, 5 and 10 wt%, respectively. Based on Fig. 8, there is an apparent linear change stage in the three curves, during which the samples undergo elastic deformation. As the load further increases, the aerogel matrix is crushed and the porous structure is destroyed. Table 4 lists the compressive properties of each sample and the comparison with the glass fiber-reinforced SiO$_2$ aerogel. When the fiber content is constant, increasing the PI content leads to increasing both Young's modulus and compression strength. This result indicates that the PI effectively strengthens the skeleton structure of SiO$_2$ and remarkably improves the resistance to deformation. The

Table 3 Pore structure parameters of FPS aerogels

Samples	Specific surface area/(m²/g)	Average pore size/nm	Pore volume/(cm³/g)
1#_PI-2 wt%_GF-1 wt%	866	14.8	3.16
2#_PI-2 wt%_GF-2 wt%	844	17.4	3.67
4#_PI-5 wt%_GF-1 wt%	913	15.4	3.52
5#_PI-10 wt%_GF-1 wt%	963	17.1	4.05
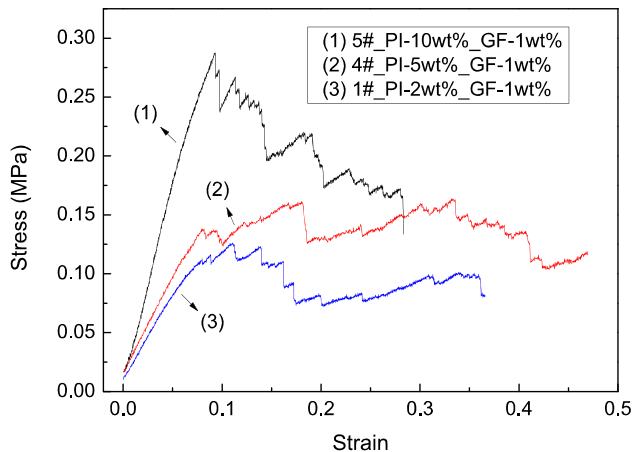
Figure 8 Compressive stress–strain curves of FPS aerogels.

compression strength and Young's modulus of the sample with 10 wt% PI are 0.29 and 3.22 MPa respectively, indicating that the compression strength is about 16 times larger compared to pure SiO_2 aerogel. In summary, the compression strength and Young's modulus of FPS aerogels are significantly improved compared to the glass fiber-reinforced SiO_2 aerogels.

As is shown in Fig. 9, the TG–DSC analysis of the FPS aerogel sample (5#_PI-10 wt%_GF-1 wt%) was performed in air from 30 to 800 °C. We can see that the first weight loss is about 4.8% from 30 to 130 °C, which corresponds to the adsorption of water and

ethanol. The second weight loss is around 3.4%, which is due to the evaporation of a small amount of NMP and the oxidation of a small amount of residual TEOS in the pore. The third weight loss (3.2%) stating at around 350 °C is attributed to degradation of the propyl groups from APTES [15]. The exothermic peak of the DSC curve at 575° C is due to the decomposition of PI, which corresponds to about 7.2% weight loss with an onset at 520 °C.

Conclusions

A lightweight FPS composite aerogel was prepared combining PI cross-linking and glass fiber reinforcement methods. The introduction of the PI significantly improved the mechanical properties of SiO_2-based aerogels and the glass fibers reduced shrinkage. The compression strength, Young's modulus and thermal conductivity of the aerogels increase with the increasing PI content. An FPS aerogel with 1 wt% fiber and 10 wt% PI was obtained with a density of 0.145 g/cm³, a shrinkage of 13.7%, a specific surface area of 963 m²/g and a thermal conductivity of 0.0282 W m⁻¹ K⁻¹. The value of the compression strength (0.29 MPa) was 16 times greater than pure SiO_2 aerogel and higher compared to the glass fiber-reinforced SiO_2 aerogel with a similar density.

Table 4 Compression properties of the FPS aerogel

Samples	Density/(g/cm³)	Strain/%	Strength/MPa	Young's modulus/MPa
1#_PI-2 wt%_GF-1 wt%	0.120	8.8	0.12	1.36
4#_PI-5 wt%_GF-1 wt%	0.132	8.0	0.14	1.75
5#_PI-10 wt%_GF-1 wt%	0.145	9.0	0.29	3.22
SiO_2 aerogel [23]	0.09	–	0.017–0.021	1
Glass fiber-reinforced SiO_2 aerogel [9]	0.120	10.0	0.05	0.5
Glass fiber-reinforced SiO_2 aerogel [10]	0.138–0.161	25.0	0.030–0.189	0.41–1.03
Glass fiber-reinforced SiO_2 aerogel [14]	0.153	20.0	0.059	0.637
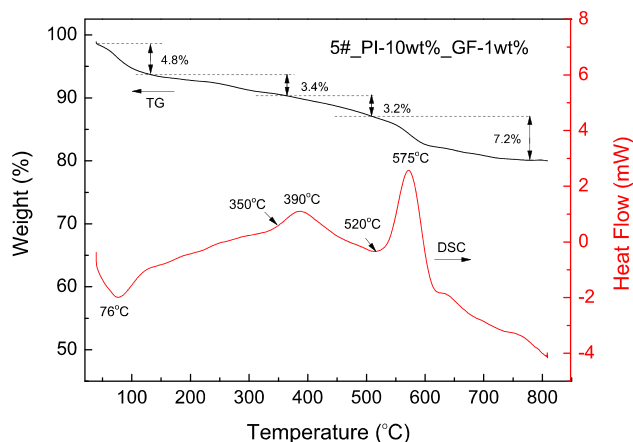
Figure 9 The TG–DSC curves of the FPS aerogel.

Acknowledgements

Compliance with ethical standards

Conflict of interest The authors declare that they have no competing interests.

References

[1] Pierre AC, Pajonk GM (2002) Chemistry of aerogels and their applications. Chem Rev 102(11):4243–4266

[2] Mohanan JL, Brock SL (2004) A new addition to the aerogel community: unsupported CdS aerogels with tunable optical properties. J Non Cryst Solids 350:1–8

[3] Koebel M, Rigacci A, Achard P (2012) Aerogel-based thermal superinsulation: an overview. J Sol–Gel Sci Technol 63:315–339

[4] Yan P, Zhou B, Du A (2014) Synthesis of polyimide cross-linked silica aerogels with good acoustic performance. RSC Adv 4(102):58252–58259

[5] Rao AV, Hegde ND, Hirashima H (2007) Absorption and desorption of organic liquids in elastic superhydrophobic silica aerogels. J Colloid Interface Sci 305(1):124–132

[6] Hæreid S, Nilsen E, Einarsrud MA (1996) Properties of silica gels aged in TEOS. J Non Cryst Solids 204(3):228–234

[7] Einarsrud MA, Kirkedelen MB, Nilsen E, Mortensen K, Samseth J (1998) Structural development of silica gels aged in TEOS. J Non Cryst Solids 231(1–2):10–16

[8] Shi M, Tang C, Yang X, Zhou J, Jia F, Han Y, Li Z (2017) Superhydrophobic silica aerogels reinforced with polyacrylonitrile fibers for adsorbing oil from water and oil mixtures. RSC Adv 7(7):4039–4045

[9] Yu Y, Wu X, Sang H (2015) Preparation and characterization of hydrophobic SiO_2-glass fibers aerogels via ambient pressure drying. J Mater Eng 43(8):31–36 **(in Chinese)**

[10] Shi X, Zhang R, He S, Li Z, Cao W, Cheng X (2016) Synthesis and heat insulation performance of glass fiber reinforced SiO_2 aerogel composites. J Chin Ceram Soc 44(1):129–135 **(in Chinese)**

[11] Wu H, Chen Y, Chen Q, Ding Y, Zhou X, Gao H (2013) Synthesis of flexible aerogel composites reinforced with electrospun nanofibers and microparticles for thermal insulation. J Nanomater 2013:1–8

[12] Markevicius G, Ladj R, Niemeyer P, Budtova T, Rigacci A (2017) Ambient-dried thermal superinsulating monolithic silica-based aerogels with short cellulosic fibers. J Mater Sci 52(4):2210–2221. https://doi.org/10.1007/s10853-016-0514-3

[13] Jiang Y, Feng J, Feng J (2017) Synthesis and characterization of ambient-dried microglass fibers/silica aerogel nanocomposites with low thermal conductivity. J Sol–Gel Sci Technol 83(1):64–71

[14] Li C, Cheng X, Li Z, Pan Y, Huang Y, Gong L (2017) Mechanical, thermal and flammability properties of glass fiber film/silica aerogel composites. J Non Cryst Solids 457:52–59

[15] Guo J, Nguyen BN, Li L, Meador MAB, Scheiman DA, Cakmak M (2013) Clay reinforced polyimide/silica hybrid aerogel. J Mater Chem A 1(24):7211–7221

[16] Yang H, Kong X, Zhang Y, Wu C, Cao E (2011) Mechanical properties of polymer-modified silica aerogels dried under ambient pressure. J Non Cryst Solids 357(19):3447–3453

[17] Maleki H, Durães L, Portugal A (2014) Synthesis of light-weight polymer-reinforced silica aerogels with improved mechanical and thermal insulation properties for space applications. Microporous Mesoporous Mater 197:116–129

[18] Saeed S, Al Soubaihi RM, White LS, Bertino MF, Saoud KM (2016) Rapid fabrication of cross-linked silica aerogel by laser induced gelation. Microporous Mesoporous Mater 221:245–252

[19] Wang Q, Feng J, Ma L et al (2016) Synthesis, characterization, and adsorption properties of silica aerogels cross-linked with diisocyanate under ambient drying. J Mater Sci 51(20):9472–9483.   https://doi.org/10.1007/s10853-016-0191-2

[20] Fei Z, Yang Z, Chen G, Li K (2018) Preparation of tetraethoxysilane-based silica aerogels with polyimide cross-

linking from 3,3′,4,4′-biphenyltetracarboxylic dianhydride and 4,4′-oxydianiline. J Sol–Gel Sci Technol 85(3):506–513

[21] Sarawade PB, Kim JK, Kim HK, Kim HT (2007) High specific surface area TEOS-based aerogels with large pore volume prepared at an ambient pressure. Appl Surf Sci 254(2):574–579

[22] Orel B, Ješe R, Vilčnik A, Štangar UL (2005) Hydrolysis and solvolysis of methyltriethoxysilane catalyzed with HCl or trifluoroacetic acid: IR spectroscopic and surface energy studies. J Sol–Gel Sci Technol 34(3):251–265

[23] Alaoui AH, Woignier T, Scherer GW, Phalippou J (2008) Comparison between flexural and uniaxial compression tests to measure the elastic modulus of silica aerogel. J Non Cryst Solids 354(40):4556–4561